RESEARCH ARTICLE

Controlling roll-yaw coupling with aileron and twist design[†]

J.R. Brincklow[1] , Z.S. Montgomery[2] and D.F. Hunsaker[3]

[1]CAEUSA, Arlington, TX, USA
[2]Area-I, Marietta, GA, USA
[3]Utah State University, Logan, UT, USA
Corresponding author: J.R. Brincklow; Email: josh.brincklow@gmail.com

Abstract
Most simple ailerons produce adverse yaw. However, with proper aileron placement and wing twist, an aileron can produce proverse or neutral yaw, eliminating the need for aileron-rudder mixing, differential aileron deflection or Frise ailerons. The relationship between wing planform, aileron placement and lift distribution is studied here for a special class of optimal lift distributions that minimise induced drag for a variety of design constraints. It is shown that a wing employing the elliptic lift distribution will always produce adverse yaw, independent of aileron design or operating condition. However, for wings employing other optimal lift distributions, the ailerons can be placed to produce proverse or neutral yaw. A numerical lifting-line algorithm is used to explore the impact of aileron design on a wide range of wing planforms and lift distributions. Results can be used in the early stages of design to correctly place ailerons with respect to desired roll-yaw coupling.

Nomenclature

A_j	Fourier coefficients used in the solution to the fundamental lifting-line equation
a_j	decomposed Fourier coefficients corresponding to wing planform shape
B_j	normalised Fourier coefficients: $B_j \equiv A_j/A_1$
b	wingspan
b_j	decomposed Fourier coefficients corresponding to spanwise symmetric twist
$\tilde{C}_{L,\alpha}$	section lift slope
C_{D_i}	induced-drag coefficient
C_L	lift coefficient
C_ℓ	rolling-moment coefficient
C_n	yawing-moment coefficient
c	local section chord length
c_j	decomposed Fourier coefficients corresponding to spanwise antisymmetric twist caused by ailerons
j	term in the Fourier sine series
N	number of terms retained when truncating the infinite Fourier sine series
R_A	aspect ratio
$R_{n/\ell}$	roll-yaw control ratio
R_T	taper ratio
s	normalised spanwise coordinate: $s = 2z/b$
s_{centre}	spanwise position of the aileron centre
s_{root}	aileron root, spanwise position of the inboard aileron edge

---

[†]This paper was presented as paper AIAA 2021-0327 at the AIAA SciTech 2021 Forum Conference (Virtual).

s_{tip}	aileron tip, spanwise position of the outboard aileron edge
s_{width}	aileron width along the semispan
V_∞	freestream velocity
z	spanwise coordinate centred at the wing root, positive out the left wing

Greek symbol

α	local geometric angle-of-attack relative to the freestream
α_{L0}	local zero-lift angle-of-attack
Γ	local circulation strength on the lifting line
δ_a	amount of aileron deflection
ε_f	local section flap effectiveness
θ	change of variables for the spanwise coordinate
χ	normalised spanwise antisymmetric twist distribution function used to describe aileron size and location
Ω	amount of the symmetric component of wing twist
ω	normalised spanwise symmetric twist distribution function

1.0 Introduction

Conventional ailerons typically produce adverse yaw. To combat this, several methods have been widely used including mixing aileron deflection with rudder deflection, applying non-antisymmetric aileron deflections, or employing specific aileron designs that increase drag when deflected upwards such as Frise ailerons [1–3]. An alternative method, which is the focus of this paper, couples particular aileron placement with a series of symmetric lift distributions designed to produce proverse yaw. The Horten brothers were allegedly the first to implement this approach on a flying wing, although literature on this can be difficult to find [4, 5]. More recently, Bowers et al. [6] have demonstrated this principle on a subscale aircraft, and Hunsaker et al. [7] have shown theoretical continuous antisymmetric twist distributions that will produce proverse yaw when coupled with a particular class of optimal symmetric lift distributions.

Simply placing an aileron in a specific location on a wing is not sufficient to ensure the production of proverse yaw. Rather, aileron placement that will result in proverse yaw depends on the symmetric lift distribution. Some lift distributions, such as the elliptic lift distribution, cannot be used with ailerons to produce proverse yaw [6–10]. However, as will be shown here, there is a class of optimal symmetric lift distributions that, when coupled with proper aileron placement, can produce proverse, adverse or neutral yaw. The particular class of optimal symmetric lift distributions that will be used in this work is the same as those studied by Phillips et al. [11–13], Taylor et al. [14, 15], and Hunsaker et al. [7, 9]. It includes several lift distributions that have been shown to minimise induced drag under a variety of aerodynamic, geometric, structural, deflection and operational constraints. This class of lift distributions includes the elliptic lift distribution, Prandtl's bell-shaped lift distribution [16], and several other distributions [11–14]. This class of analytic lift distributions has been shown to match high-fidelity aero-structural optimisation studies performed computationally and experimentally as shown by Taylor [15].

The method of producing proverse yaw by coupling the lift distribution with aileron placement can be particularly useful for flying-wing designs that do not have a rudder control surface, and can be considered bio-inspired since there is evidence that birds can produce proverse yaw in a similar manner [6]. Additionally, these methods can be particularly important for high-aspect-ratio wings that use a non-elliptic lift distribution to reduce structural weight and wing deflection [11–14]. Finally, a more thorough understanding of this approach can be useful for designing future tailless aircraft.

The symmetric lift distribution produced on a finite wing depends on the wing planform and washout distribution. The relationship between planform, twist, lift distribution and the resulting integrated forces

and moments on a finite wing are well understood and have been studied since the development of lifting-line theory in the early 20th century [17–25]. Theoretical relationships for roll-yaw coupling are first developed using classical lifting-line theory. A numerical analogue to this theory is then used to compute aileron placement that will produce desired roll-yaw coupling over a wide range of planforms and optimal lift distributions. The resulting data and analysis can be used in early stages of aircraft design for aircraft intending to control roll-yaw coupling with aileron placement. It should be noted that the computational solutions included in the Results section were computed assuming an aerofoil lift slope of $\tilde{C}_{L,\alpha} = 2\pi$. Since many common aerofoils have a lift slope close to this value, the results shown here are a reasonable approximation for many applications. However, blended-body flying-wing designs often implement thick aerofoils near the wing root. Since effects of thickness were not directly studied, results presented in this paper should be used with caution for blended-body configurations.

2.0 Analytic formulation

Prandtl's classical lifting-line theory [17, 18] has formed the basis of our understanding of wing design for the past century. Solutions to the fundamental lifting-line equation are obtained by assuming a circulation distribution Γ that can be written in terms of a Fourier sine series as

$$\Gamma(\theta) = 2bV_\infty A_1 \left(\sin(\theta) + \sum_{j=2}^{\infty} B_j \sin j\theta \right), \theta \equiv \cos^{-1}(-2z/b), B_j \equiv A_j/A_1 \tag{1}$$

where b is the wing span, V_∞ is the freestream velocity, A_j are the Fourier coefficients, B_j are normalised Fourier coefficients and θ is a change of variables related to the spanwise location z. The Fourier coefficients A_j are obtained by forcing the lifting-line equation to be satisfied at a finite number of (N) locations along the wing. This gives a linear system of equations that can be solved for the truncated Fourier series

$$\sum_{j=1}^{N} A_j \left(\frac{4b}{\tilde{C}_{L,\alpha} c(\theta)} + \frac{j}{\sin(\theta)} \right) \sin(j\theta) = \alpha(\theta) - \alpha_{L0}(\theta) \tag{2}$$

where $\tilde{C}_{L,\alpha}$ is the aerofoil section lift slope, c is the local section chord, α is the local section geometric angle-of-attack, and α_{L0} is the local section zero-lift angle-of-attack. The integrated lift, induced-drag, rolling-moment and yawing-moment coefficients on the wing in the absence of rolling rate can be computed from the resulting Fourier coefficients [26, 27]

$$C_L = \pi R_A A_1 \tag{3}$$

$$C_{D_i} = \frac{C_L^2}{\pi R_A} \left(1 + \sum_{j=2}^{N} j B_j^2 \right) \tag{4}$$

$$C_\ell = -\frac{1}{4} C_L B_2 = -\frac{1}{4} \pi R_A A_2 \tag{5}$$

$$C_n = -\frac{C_L^2}{4\pi R_A} \left(\sum_{j=2}^{N} (2j-1) B_{j-1} B_j \right) \tag{6}$$

where R_A is the wing aspect ratio defined as $R_A \equiv b^2/S_w$ and S_w is the wing area.

An alternative form of lifting-line theory has been presented [26] that decouples the effects of angle-of-attack, washout and aileron deflection. This method has been used to develop significant insight into the optimum washout distributions and will be used here to consider optimum aileron placement. In a theoretical sense, the deflection of an aileron is simply a step-change in aerodynamic twist, since a

Table 1. *Optimal lift distributions for various structural constraints*

	B_3	Constraints
a	$-1/3$	Fixed gross weight and moment of inertia of lift
	$-1/3$	Fixed net weight, maximum stress, and stall speed
b	-0.17715	Fixed net weight, maximum deflection, and stall speed
c	$-3/8 + \sqrt{9/64 - 1/12}$	Fixed gross weight, maximum stress, and wing loading
d	$-3/7 + \sqrt{9/49 - 1/21}$	Fixed gross weight, maximum deflection, and wing loading

deflection changes the section zero-lift angle-of-attack but produces very little change in the section lift slope. Here we apply the change of variables

$$B_j = \frac{\pi R_A}{C_L} \left[a_j (\alpha - \alpha_{L0})_{\text{root}} + b_j \Omega + c_j \delta_a \right] \qquad (7)$$

where a_j, b_j, and c_j are decomposed Fourier coefficients, Ω is the amount of symmetric wing twist, and δ_a is the aileron deflection, or the amount of antisymmetric twist. The three components on the right-hand side of Equation (7) are the contributions of angle-of-attack and planform, spanwise-symmetric twist (washout) and spanwise-antisymmetric twist caused by an aileron deflection. Considering only wings with symmetric planforms and noting from Equation (2) that only odd Fourier coefficients depend on symmetric components and only even coefficients depend on antisymmetric components, Equation (7) can be expressed as

$$B_j = \frac{\pi R_A}{C_L} \begin{cases} a_j (\alpha - \alpha_{L0})_{\text{root}} + b_j \Omega & j \text{ odd} \\ c_j \delta_a & j \text{ even} \end{cases} \qquad (8)$$

The decomposed Fourier coefficients a_j, b_j and c_j can be obtained from

$$\sum_{j=1}^{N} a_j \left(\frac{4b}{\tilde{C}_{L,\alpha} c(\theta)} + \frac{j}{\sin(\theta)} \right) \sin(j\theta) = 1 \qquad (9)$$

$$\sum_{j=1}^{N} b_j \left(\frac{4b}{\tilde{C}_{L,\alpha} c(\theta)} + \frac{j}{\sin(\theta)} \right) \sin(j\theta) = \omega(\theta) \qquad (10)$$

$$\sum_{j=1}^{N} c_j \left(\frac{4b}{\tilde{C}_{L,\alpha} c(\theta)} + \frac{j}{\sin(\theta)} \right) \sin(j\theta) = \varepsilon_f(\theta) \, \chi(\theta) \qquad (11)$$

where $\omega(\theta)$ is a normalised symmetric twist distribution function (washout distribution), $\chi(\theta)$ is a normalised antisymmetric twist distribution function caused by the ailerons, and $\varepsilon_f(\theta)$ is the section flap effectiveness of the ailerons [27].

We will limit this study to a special class of optimum symmetric lift distributions given by $B_j = 0$ for all odd terms $j > 3$ [7, 9, 11–14, 16]. This class of lift distributions provides the minimum induced drag for various aerodynamic and structural design constraints [11–14, 16–18] and is fully defined by the single parameter B_3. For example, an elliptic lift distribution is defined by $B_3 = 0$, and Prandtl's bell-shaped lift distribution is defined by $B_3 = -1/3$. Other optimal lift distributions minimising induced drag for various design and operating constraints exist within the range $-1/3 < B_3 < 0$ and are shown in Table 1 along with their associated structural and aerodynamic constraints [11–14, 16–18, 26].

For a wing of arbitrary planform to produce a prescribed lift coefficient and lift distribution within this class of optimal lift distributions, the symmetric dimensionless twist distribution, twist amount and angle-of-attack must be [12]

$$\omega(\theta) = \frac{4b/\tilde{C}_{L,\alpha}\left[(1 - B_3)/c_{\text{root}} - \left[\sin(\theta) + B_3\sin(3\theta)\right]/c(\theta)\right] - 3B_3\left[1 + \sin(3\theta)/\sin(\theta)\right]}{4b(1 - B_3)/\left(\tilde{C}_{L,\alpha}c_{\text{root}}\right) - 12B_3} \quad (12)$$

$$\Omega = \frac{C_L}{\pi R_A}\left(\frac{4b(1 - B_3)}{\tilde{C}_{L,\alpha}c_{\text{root}}} - 12B_3\right) \quad (13)$$

$$(\alpha - \alpha_{L0})_{\text{root}} = \frac{C_L}{\pi R_A}\left(\frac{4b(1 - B_3)}{\tilde{C}_{L,\alpha}c_{\text{root}}} + 1 - 3B_3\right) \quad (14)$$

The normalised twist distribution function due to aileron placement can be written as [27]

$$\chi(s) \equiv \begin{cases} 0, & s < -s_{\text{tip}} \\ 1, & -s_{\text{tip}} \leq s < -s_{\text{root}} \\ 0, & -s_{\text{root}} \leq s \leq s_{\text{root}} \\ -1, & s_{\text{root}} < s \leq s_{\text{tip}} \\ 0, & s_{\text{tip}} < s \end{cases} \quad (15)$$

where s is a normalised spanwise coordinate $s \equiv 2z/b$, and s_{root} and s_{tip} are the spanwise locations corresponding to the aileron edges closest to the wing root and wing tip and will be called the aileron root and aileron tip respectively. These two design variables s_{root} and s_{tip} can be altered to consider their effect on roll-yaw coupling for this class of symmetric lift distributions.

From Equations (5) and (8) it can be seen that only the c_2 component of the aileron contributes to the rolling-moment coefficient

$$C_\ell = -\frac{1}{4}\pi R_A c_2 \delta_a \quad (16)$$

By inspection of Equations (4), (8), and (11), the $\chi(\theta)$ design that minimises induced drag requires $c_j = 0$ for $j > 2$ [10]. Such a design requires continuous antisymmetric twist [28–39] and is not possible with the discrete aileron deflection distribution defined in Equation (15). Effects of discrete aileron placement on induced drag have been considered by Feifel [40] and Brincklow et al. [41]. From Equation (6) we see that the yawing-moment depends on the product of neighbouring Fourier coefficients $B_{j-1}B_j$. This fact combined with the definition of the class of symmetric lift distributions considered in this work means that only the c_2 and c_4 components of the aileron contribute to the yawing-moment coefficient. From Equations (6) and (8) the yawing-moment coefficient can be written as

$$C_n = \frac{1}{4}C_L\delta_a[(3 + 5B_3)c_2 + 7B_3c_4] \quad (17)$$

Equations (16) and (17) can be combined to give the *roll-yaw control ratio* [7]

$$R_{n/\ell} \equiv \frac{C_n}{C_L C_\ell} = -\frac{1}{\pi R_A}\left(3 + 5B_3 + 7B_3\frac{c_4}{c_2}\right) \quad (18)$$

Equation (18) provides important insight into the design of wings for prescribed roll-yaw coupling. Notice that for $B_3 = 0$ (the elliptic lift distribution), the roll-yaw coupling will always be negative and equal to

$$R_{n/\ell} = \frac{-3}{\pi R_A} \quad (19)$$

This relationship was first published by Munk [42] and demonstrates that the elliptic lift distribution will always produce adverse yaw, independent of the aileron design or placement. However, Equation (18) also shows that for any lift distribution defined by a non-zero value for B_3, the roll-yaw coupling depends on the ratio of the decomposed Fourier coefficients c_4/c_2, which are both related to the aileron design. For $B_3 < 0$, if $c_4/c_2 < -(3 + 5B_3)/(7B_3)$, the wing will produce adverse yaw;

if $c_4/c_2 = -(3 + 5B_3)/(7B_3)$, the wing will produce neutral yaw, and if $c_4/c_2 > -(3 + 5B_3)/(7B_3)$, the wing will produce proverse yaw. The decomposed Fourier coefficients c_2 and c_4 are not independent parameters that can be varied directly. Rather they depend on the wing planform and aileron design through Equations (11) and (15). Even so, Equation (18) provides a strong theoretical foundation demonstrating that proverse yaw is possible for many lift distributions with proper aileron design.

Equation (18) provides additional important insight into the dependence of the roll-yaw control ratio on wing design and operating conditions. Note that the right-hand side of Equation (18) is completely independent of the wing operating condition, including angle-of-attack, lift coefficient or rolling-moment coefficient. Additionally, from Equation (11), it can be shown that c_2 and c_4 are both dependent on aileron design, but independent of aileron deflection magnitude. Hence the roll-yaw control ratio is independent of the aileron deflection magnitude. The right-hand side of Equation (18) does depend on the wing aspect ratio, lift distribution B_3, wing planform and aileron design. In the following analysis, operating conditions and aileron deflections were chosen out of necessity to produce solutions. As will be illustrated, the results for the roll-yaw control ratio shown for a range of wing planforms, aspect ratios, lift distributions and aileron designs in the following sections are independent of operating condition or aileron deflection magnitude below stall.

Numerical methods could be employed to solve the infinite-series solution to the lifting-line development shown here and correlate the wing and aileron geometry to solutions for c_2 and c_4. However, this classical lifting-line development is best solved using cosine clustering, which is limited in how well the discrete changes in twist due to aileron deflection can be resolved [41]. Therefore, in the remainder of this work, a modern numerical lifting-line algorithm developed by Phillips and Snyder [43] is used, which is a numerical analogue to the classical lifting-line theory but allows for grid clustering in areas of high gradients. In this way, the step-change in twist distribution due to aileron deflection can be properly resolved.

3.0 Numerical method

The numerical lifting-line algorithm of Phillips and Snyder [43], similar to classical lifting-line theory, assumes that the section lift coefficient at any given spanwise location along the lifting surface is equivalent to the 2D case at the same local angle-of-attack. Because of this, the algorithm works best for wings with aspect ratio of four or greater, where spanwise flow effects are minimal. The numerical algorithm shows good agreement with higher fidelity aerodynamic tools and experimental results [43], and has been implemented in several journal publications [10, 41, 44–49]. The particular implementation of the numerical lifting-line algorithm used in this work is an open-source tool called MachUp [43, 49], which allows control points to be clustered at the wing tips as well as near the aileron edges. MachUp was used here to evaluate the effect of aileron placement on the resulting yawing moment for a large range of planforms and B_3 lift distributions.

A grid resolution study was performed for the case of $R_A = 8, R_T = 1, B_3 = -1/3, C_L = 0.5, C_\ell = 0.1$, $s_{\text{root}} = 0.5$, and $s_{\text{tip}} = 0.9$. Figure 1 shows the induced drag coefficient and roll-yaw control ratio results for this study for increasing node count. For reference, the classical lifting-line results are also shown for varying truncation points of the infinite series solution. Results from this study show that using 100 nodes along each wing semispan in the MachUp simulations gives grid-resolved solutions. For this study and the following results, the nodes were distributed using cosine clustering across the inboard section of the wing, the aileron section, and the outboard section. The number of nodes used along each wing section was proportional to the spanwise length of that section divided by the wing semispan. For example, if the aileron covered 20% of the spanwise length of the wing, 20 nodes were used on that section. The aileron flap-chord fraction is unity for all cases in this study. However, as Feifel [40] notes, the flap-chord fraction does not affect the induced drag predicted by potential-flow algorithms, and only affects the aileron deflection magnitude. As discussed earlier and demonstrated in Equation (18), the aileron deflection has no influence on the roll-yaw control ratio.
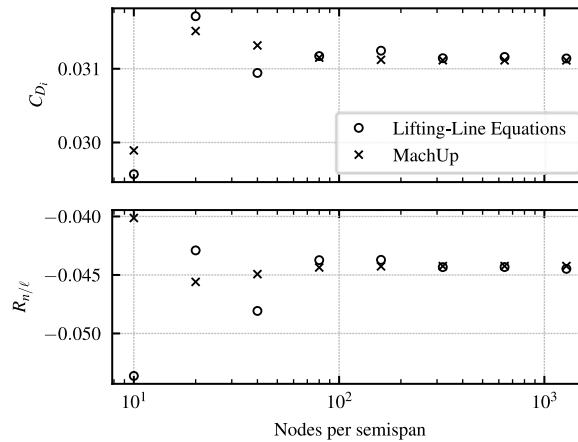
**Figure 1.** *Grid resolution of MachUp and classical lifting-line theory.*
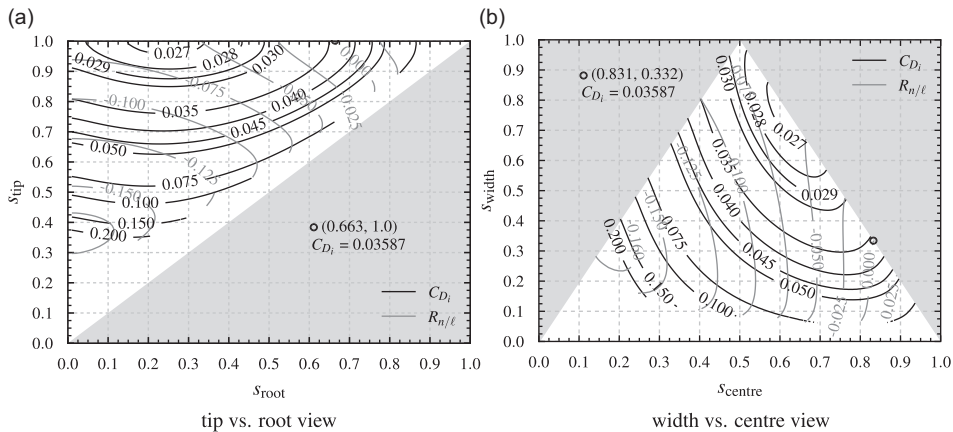
Figure 2. *Induced-drag and roll-yaw control ratio contours.*

The class of lift distributions included in this study are completely defined by the single parameter B_3. For a given planform, lift coefficient, rolling-moment coefficient and lift distribution defined by B_3, the washout distribution, washout magnitude, and root angle-of-attack were computed from Equations (12)–(14) and employed in the MachUp simulation. A Newton-Secant method was used to find the aileron deflection that would produce the prescribed rolling moment, and the resulting induced drag and yawing moment as predicted by MachUp were recorded. From these results, the roll-yaw control ratio $R_{n/\ell}$ was computed from the definition given in (18). This process was repeated over a wide range of wing planform shapes and aileron placement. For the results presented in this study, $\varepsilon_f\,(\theta)$ was set to 1.0 for all wing sections with an aileron, and the section lift slope was set to the theoretical value from thin-aerofoil theory, $\tilde{C}_{L,\alpha} = 2\pi$.

Figure 2 shows example results for the induced-drag coefficient and roll-yaw control ratio for a rect-angular wing with $R_A = 8$, $B_3 = -1/3$, $C_L = 0.5$, and $C_\ell = 0.1$. Figure 2 includes two plots that show contours of the induced-drag coefficient and roll-yaw control ratio as a function of the aileron spanwise size and location. Figure 2(a) shows the view with respect to s_{root} and s_{tip} while Fig. 2(b) shows the data with respect to the aileron centre $s_{\text{centre}} = \left(s_{\text{root}} + s_{\text{tip}}\right)/2$ and aileron width $s_{\text{width}} = s_{\text{tip}} - s_{\text{root}}$. Note that the shaded regions are blank since they represent infeasible aileron designs. All results only assume
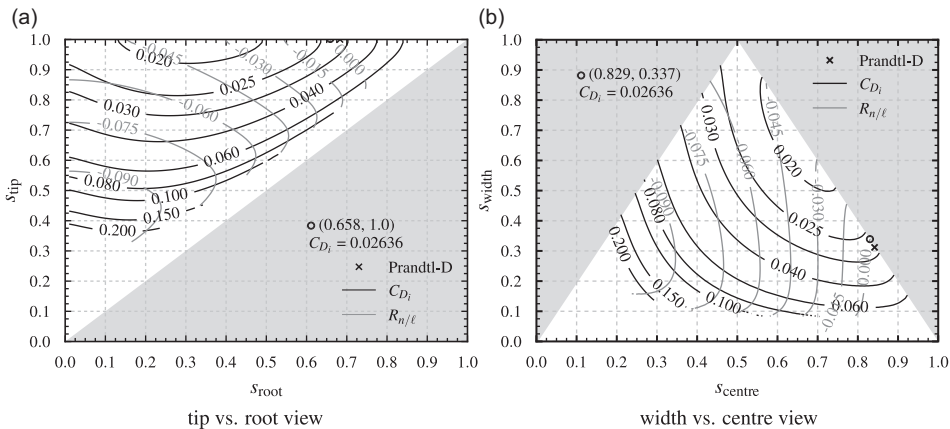
Figure 3. *Induced-drag and roll-yaw control ratio contours for a Prandtl-D-like wing planform [6].*

inviscid conditions and do not include the effects of stall. As will be shown, these results are independent of aileron deflection and operating condition below stall. Notice the nearly vertical contour with a noted $R_{n/\ell} = 0$ near a s_{centre} of 0.825 in Fig. 2(b). This contour line represents the range of aileron widths that can be used to produce zero roll-yaw coupling, and indicates that an aileron centred at the spanwise location $s = 0.825$ will produce neutral yaw for this design. In general, an aileron with the centre inboard of this location will produce adverse yaw, and an aileron with the centre outboard of this location will produce proverse yaw, regardless of aileron width. The contours for induced drag demonstrate that in general, the induced drag decreases with increasing aileron size along lines of constant roll-yaw control ratio. Therefore, if we wish to minimise induced drag, we should select an aileron that extends to the wing tip. The case that corresponds to this minimum-induced-drag solution for a design with $R_{n/\ell} = 0$ is marked with a circle in Fig. 2.

Figure 3 shows similar data based on the planform of the Prandtl-D aircraft created by NASA [6] with $R_A = 15.55$ and a taper ratio $R_T = 0.26$. NASA's Prandtl-D wing is an experimental aircraft, which showed Prandtl's bell-shape wing lift distribution combined with careful aileron design is capable of producing proverse yaw. Research [6] supports that this lift distribution is more similar to avian flight compared to the elliptical lift distribution. The design of the aircraft planform is a quarter-scale of the Horten H Xc aircraft; the aircraft has no vertical surfaces, and has elevons starting at 86% of the wing semi-span and continuing to the wing tip [6]. For more information about the design, manufacturing, flight-testing and results of this aircraft, the reader is referred to the following publications [6, 50, 51]. This can be examined in a theoretical sense by considering the data in Fig. 3. The point marked with an 'x' represents the aileron design used on the Prandtl-D aircraft. Results shown in this figure predict that the aileron placement on the Prandtl-D will in fact produce proverse yaw and minimise induced drag for that roll-yaw control ratio. Additionally, the aileron design that would produce zero roll-yaw coupling and minimise induced drag is marked with a circle.

Equation (18) shows that the roll-yaw control ratio is theoretically independent of operating condition, including lift coefficient, rolling moment and aileron deflection magnitude. To verify this numerically, a single wing planform and lift distribution were chosen, and studied over a range of operating conditions. The wing planform and lift distribution used in this study were the same as those used to produce the results in Fig. 2. Two aileron designs were considered for this wing planform and lift distribution. The first was a somewhat arbitrary aileron design defined by $s_{root} = 0.5$ and $s_{tip} = 0.9$. From the results in Fig. 2, that aileron design was expected to produce adverse yaw. The second aileron design was specifically chosen as the design that produces a neutral roll-yaw control ratio and minimises induced drag, and is defined by $s_{root} = 0.663$ and $s_{tip} = 1.0$. For each aileron design, the operating lift coefficient C_L was varied from 0.001 to 1.0 using 10 equally spaced points, and the operating rolling-moment
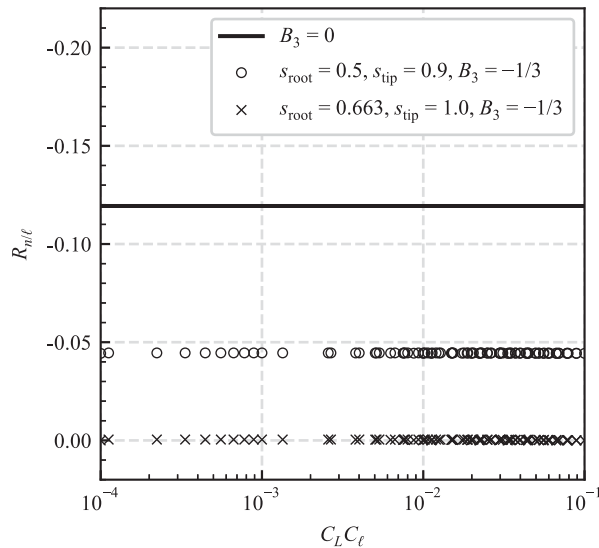
Figure 4. *Roll-yaw control ratio results for a range of operating conditions.*

coefficient C_ℓ was varied from 0.001 to 0.1 using 10 equally spaced points. Each combination of lift coefficient and rolling-moment coefficient was considered as an individual case, which gave 100 total cases for each aileron design. In each case, the required aileron deflection was found and the resulting yawing moment and corresponding roll-yaw control ratio was obtained. Figure 4 shows results of the study. Notice that the roll-yaw control ratio for each aileron design is independent of the operating condition and aileron deflection. This substantiates the theoretical solution given in Equation (18). Also included in the figure for comparison are the analytic results for an elliptic lift distribution on a wing with the same aspect ratio, as given in Equation (19).

4.0 Results

Using the numerical algorithm presented in Section 3 and our understanding of the aileron design space, we now consider the aileron design required to produce a desired roll-yaw coupling over a range of planforms and symmetric lift distributions. To be able to predict the roll-yaw coupling of a given aileron geometry, we simply need to find the aileron design that will produce zero roll-yaw coupling. Any aileron inboard of that location will produce adverse yaw, and any aileron outboard of that location will produce proverse yaw. Since, in general, there are multiple solutions for aileron designs that produce zero roll-yaw coupling for a given wing planform and lift distribution, we wish to select the aileron design that will minimise induced drag. Notice that for the cases shown in Figs. 2 and 3, the induced drag is minimised by selecting an aileron that extends to the tip, i.e. $s_{tip} = 1$. Repeating this analysis for wing designs in the range: $-0.5 \leq B_3 < 0, 4 \leq R_A \leq 20, 0 \leq R_T \leq 1$ and various C_ℓ values, it was determined that each aileron design within this range that gives zero roll-yaw control ratio and minimum induced drag has $s_{tip} = 1$. Therefore, in the results that follow, the aileron tip was fixed at the tip, and only the aileron root, s_{root}, was allowed to vary.

The aileron root position that would provide a zero roll-yaw control ratio for each case was found using the gradient-based optimisation code Optix [49], which employs the BFGS algorithm [52–55]. Because MachUp uses a finite number of control points per semispan, with small changes to s_{root}, the distribution of control points between the ailerons and regular wing sections can change causing step changes in the solution. This was resolved with an iterative process of running Optix with a fixed nodal distribution between aileron sections and regular wing sections. Once a converged solution was obtained,
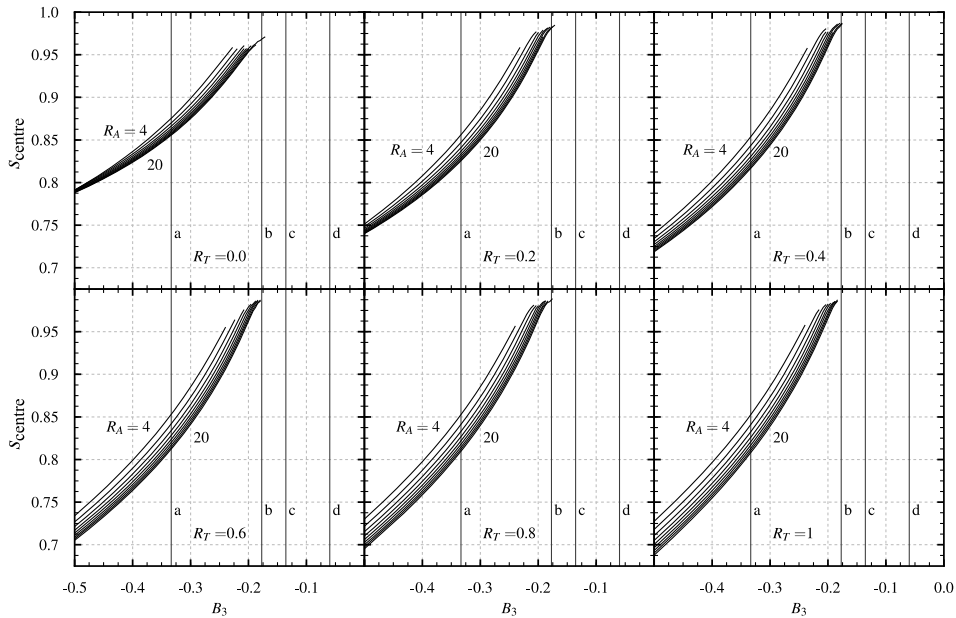
Figure 5. *Aileron centre location shown as a function of B_3 for neutral roll-yaw coupling at $s_{\text{tip}} = 1$.*

the nodal distribution was altered to reflect the new ratio of aileron span to wing span, and the optimisation code was run again. This process was repeated in an outer loop until the location of the aileron stopped changing. The optimisation solutions that resulted in a final roll-yaw control ratio with magnitude greater than $1.0E - 9$ were considered as designs that have no solution, and were discarded. In those cases, for the given B_3 and planform there is not an aileron design with $\varepsilon_f(\theta) = 1$ of the form in Equation (15) that can give a neutral roll-yaw control ratio. These scenarios were only encountered for B_3 values near 0. It is possible that other aileron designs, like multi-segmented ailerons, which have more degrees of freedom, could achieve zero roll-yaw control ratio at B_3 values nearer to 0. This is because an aileron design with more degrees of freedom would be better able to control the term c_4/c_2 in Equation (18). As the degrees of freedom of the aileron increase, $\varepsilon(\theta)\,\chi(\theta)$ would approach the absolute optimal solution for minimum induced drag for a given roll-yaw control ratio [7].

Resulting solutions for the aileron centre locations that give a zero roll-yaw control ratio are shown in Fig. 5 as a function of B_3 over a wide range of aspect ratios and taper ratios at the condition $C_L = 0.5$ and $C_\ell = 0.01$. Neutral lines for wings of aspect ratios from 4 to 20 in increments of 2 are shown, where the neutral line represents a band of designs providing neutral roll-yaw coupling $R_{n/\ell} = 0$ with $s_{\text{tip}} = 1$.

Any aileron design centre below the neutral line shown in Fig. 5 will produce adverse yaw, while any aileron design centre above the neutral line will produce proverse yaw. In all cases, it is assumed that the aileron extends to the wing tip. Note that as the value of B_3 decreases, solutions that produce proverse yaw can be found further inboard. Also note that as the B_3 value approaches zero (the elliptic lift distribution), solutions no longer exist. The B_3 values marked by the vertical lines labeled (a)–(d) correspond to the values in Table 1.

From Fig. 2(a) and (b) we observed that the contours of neutral roll-yaw coupling were nearly vertical when plotted as a function of the aileron centre. Therefore, if the designer wishes to design an aileron to control roll-yaw coupling and does not wish to extend the aileron to the wing tip, this can be achieved as long as the centre of the aileron remains in the correct location. The reader is reminded that maximising aileron width while not changing the aileron centre location will minimise induced drag caused by the ailerons.

5.0 Conclusion

The present work shows that it is possible to design for a certain roll-yaw control ratio through specific spanwise symmetric twist and aileron design without the need of aileron-rudder mixing, differential aileron deflection or Frise ailerons. With proper design, a wing could be developed to give neutral or proverse yaw when the ailerons are deflected. The present study has been limited to wings employing a special class of symmetric lift distributions fully defined by the parameter B_3. This class of lift distributions includes multiple analytic solutions that minimise induced drag from the wing when structural and design constraints are considered. For an arbitrary wing planform and desired lift distribution defined by B_3, the twist distribution and angle-of-attack that achieves this desired lift distribution is given by Equations (12)–(14). The resulting roll-yaw control ratio for a given planform and lift distribution depends on the aileron placement. However, it was found that any wing employing the elliptic lift distribution will produce adverse yaw independent of the aileron design. Example design spaces for aileron parameters and the resulting roll-yaw control ratio and induced drag are shown in Figs 2 and 3. It was found that the aileron designs that minimise induced drag for a given roll-yaw control ratio generally extend to the wing tip.

An optimisation routine was used in conjunction with a numerical lifting-line algorithm to find the aileron design that would minimise induced drag and ensure a roll-yaw control ratio of zero for a wide range of planforms and lift distributions within this class of distributions. The aileron centre was recorded for each solution, and plotted in Fig. 5, which shows aileron designs as a function of B_3 for various wing planforms that give zero roll-yaw control ratio while minimising induced drag. For the design space shown in Fig. 5, the aileron designs that minimised induced drag all extend to the wing tip. Any aileron that extends to the tip and has a centre location further outboard than the neutral line shown in Fig. 5 will produce proverse yaw, while a design with a centre location further inboard than the neutral line will produce adverse yaw.

This method of aileron and wing design seem particularly well suited to sailplanes and gliders, which require extreme aerodynamic efficiency while overcoming challenges caused by high-aspect-ratio wings. Some of these challenges are balancing structure weight with allowable wing bending and overcoming significant adverse yaw. The special class of lift distributions included in this study includes solutions that minimise induced drag.

Single-segment aileron designs have limitations on the obtainable roll-yaw control ratio because of their dependence on wing planform and B_3. More complex aileron designs, like multi-segmented ailerons, with more degrees of freedom could also be used to control roll-yaw coupling, and is a topic of future work.

References

[1] Abzug, M.J. and Larrabee, E.E. Rudder lock and dorsal fins, in *Airplane Stability and Control: A History of the Technologies that Made Aviation Possible*, 2nd ed, Cambridge University Press, 2005, New York, pp 221–223.

[2] Phillips, W.F. Other control surface configurations, in *Mechanics of Flight*, 2nd ed, Wiley, 2010, Hoboken, NJ, pp 682–693.

[3] Phillips, W.F. The steady coordinated turn, in *Mechanics of Flight*, 2nd ed, Wiley, 2010, Hoboken, NJ, pp 319–337.

[4] Horten, R. Lift distribution on a flying-wing aircraft, *Tech. Soaring*, 1986, **10**, (4), pp 60–61.

[5] Bowers, A. The Horten HX series: Ultralight flying wing sailplanes, TWITT Presentation, El Conjon, CA, 1998.

[6] Bowers, A.H., Murillo, O.J., Jensen, R., Eslinger, B. and Gelzer, C. On Wings of the Minimum Induced Drag: Spanload Implication for Aircraft and Birds, NASA TP-2016-219072, March 2016.

[7] Hunsaker, D.F., Montgomery, Z.S. and Joo, J.J. Adverse-yaw control during roll for a class of optimal lift distributions, *AIAA J.*, 2020, **58**, (7), https://doi.org/10.2514/1.J059038

[8] Nickel, K.L.E. Minimal Drag for Wings with Prescribed Lift, Roll Moment, and Yaw Moment, Univ. of Wisconsin-Madison Mathematics Research Center (MRC) Technical Summary Rept. 2573, September 1983, Madison, Wisconsin.

[9] Hunsaker, D.F., Moorthamers, B. and Joo, J.J. Minimum-series twist distributions for yawing-moment control during pure roll, *ZAMM*, 2021, **101**, (10), https://doi.org/10.2514/6.2019-2917

[10] Hunsaker, D.F., Montgomery, Z.S. and Joo, J.J. Analytic and computational analysis of wing twist to minimize induced drag during roll, *Proc. Inst. Mech. Eng. Part G J. Aerospace Eng.*, 2020, **234**, (3), https://doi.org/10.1177/0954410019886939

[11] Phillips, W.F., Hunsaker, D.F., and Joo, J.J. Minimizing induced drag with lift distribution and wingspan, *J. Aircraft*, 2019, **56**, (2), pp 431–441, https://doi.org/10.2514/1.C035027

[12] Phillips, W.F. and Hunsaker, D.F. Designing wing twist or planform distributions for specified lift distributions, *J. Aircraft*, 2019, **56**, (2), pp 847–849, https://doi.org/10.2514/1.C035206

[13] Phillips, W.F., Hunsaker, D.F. and Taylor, J.D. Minimizing induced drag with weight distribution, lift distribution, wingspan, and wing-structure weight, AIAA Aviation 2019 Forum, American Institute of Aeronautics and Astronautics, June 2019, https://doi.org/10.2514/6.2019-3349

[14] Taylor, J.D. and Hunsaker, D.F. Minimum induced drag for tapered wings including structural constraints, *J. Aircraft*, 2020, **57**, (4), pp 1–5.

[15] Taylor, J.D. and Hunsaker, D.F. Comparison of theoretical and multifidelity optimum aerostructural solutions for wing design, *J. Aircraft Art. Adv.*, 2021, https://doi.org/10.2514/1.C036374

[16] Prandtl, L. Uber Tragflügel kleinsten induzierten Widerstandes, *Zeitschrift fur Flugtechnik und Motorluftschiffahrt*, 1933, **24**, (11), pp 305–306.

[17] Prandtl, L. Tragflügel Theorie, Nachricten von der Gesellschaft der Wissenschaften zu Göttingen, Geschäeftliche Mitteilungen, Klasse, 1918, pp 451–477.

[18] Prandtl, L. Applications of Modern Hydrodynamics to Aeronautics, NACA TR-116, June 1921.

[19] Aldana, E.B., Mendez, A. and Lone, M. Closer look at the flight dynamics of wings with non-elliptic lift distributions, AIAA SciTech 2020 Forum, Orlando, FL, January 2020, https://doi.org/10.2514/6.2020-0284

[20] O'Donnell, R. and Mohseni, K. Roll control of low-aspect-ratio wings using articulated winglet control surfaces, *J. Aircraft*, 2019, **56**, (2), https://doi.org/10.2514/1.C034704

[21] Marquez, R.C., Monnier, J.C., Tanguy, G., Couliou, M., Brion, V. and Dupont, P. An experimental study of trailing vortex dynamics on cruise and high-lift wing configurations, AIAA Aviation 2022 Forum, Chicago, IL and Virtual, June-July 2022, https://doi.org/10.2514/6.2022-3390

[22] Klaproth, T., Bäuerle, H. and Hornung, M. Multi-fidelity aerodynamics modeling in a mission-based conceptual uav design process, AIAA Aviation 2022 Forum, Chicago, IL and Virtual, June-July 2022, https://doi.org/10.2514/6.2022-3739

[23] Pricker, I. and Armanini, S.F. Modeling, simulation and control of a tailsitter tiltrotor MAV, AIAA Scitech 2023 Forum, National Harbor, MD and Online, January 2023, https://doi.org/10.2514/6.2023-0338

[24] Richter, J., Woodring, J., Fox, S. and Agarwal, R.K. Performance study of a tapered flying wing with bell-shaped lift distribution, AIAA Scitech 2021 Forum, Virtual, January 2021, https://doi.org/10.2514/6.2021-0461

[25] Kaminski, C. and Kinzel, M. CFD investigation of the three-dimensional lift distribution of a FanWing, AIAA Scitech 2022 Forum, San Diego, CA and Virtual, January 2022, https://doi.org/10.2514/6.2022-0125

[26] Phillips, W.F. Analytical decomposition of wing roll and flapping using lifting-line theory, *J. Aircraft*, 2014, **51**, (3), pp 761–778.

[27] Phillips, W.F. Incompressible flow over finite wings, in *Mechanics of Flight*, 2nd ed, Wiley, 2010, Hoboken, NJ, pp 46–93.

[28] Joo, J.J, Marks, C., Zientarski, L. and Culler, A. Variable camber compliant wing – design, 23rd AIAA/AHS Adaptive Structures Conference, Kissimmee, FL, January 2015, https://doi.org/10.2514/6.2015-1050

[29] Marks, C.R., Zientarski, L., Culler, A.J., Hagen, B., Smyers, B.M. and Joo, J.J. Variable camber compliant wing – wind tunnel testing, 23rd AIAA/AHS Adaptive Structures Conference, Kissimmee, Florida, January 2015, https://doi.org/10.2514/6.2015-1051

[30] Miller, S.C., Rumpfkeil, M.P. and Joo, J.J. Fluid-structure interaction of a variable camber compliant wing, 53rd AIAA Aerospace Sciences Meeting, Kissimmee, FL, January 2015, https://doi.org/10.2514/6.2015-1235

[31] Joo, J.J., Marks, C.R. and Zientarski, L. Active wing shape reconfiguration using a variable camber compliant wing system, 20th International Conference on Composite Materials, Copenhagen, Denmark, July 2015.

[32] Marks, C.R., Zientarski, L. and Joo, J.J. Investigation into the effect of shape deviation on variable camber compliant wing performance, 24th AIAA/AHS Adaptive Structures Conference, San Diego, CA, January 2016, https://doi.org/10.2514/6.2016-1313

[33] Kudva, J., Appa, K., Martin, C., Jardine, A., Sendeckyj, G., Harris, T., McGowan, A. and Lake, R. Design, fabrication, and testing of the DARPA/Wright lab smart wing wind tunnel model, 38th Structures, Structural Dynamics, and Materials Conference, Kissimmee, FL, 1997, https://doi.org/10.2514/6.1997-1198

[34] Gilbert, W.W. Development of a mission adaptive wing system for a tactical aircraft, Aircraft Systems Meeting, Aircraft Design and Technology Meeting, Anaheim, CA, 1980.

[35] Hall, J.M. Executive Summary AFTI/F-111 Mission Adaptive Wing, WRDC-TR-89-2083, September 1989.

[36] Hetrick, J., Osborn, R., Kota, S., Flick, P. and Paul, D. Flight testing of mission adaptive compliant wing, 48th AIAA/ASME/ASCE/AHS/ASC Structures, Structural Dynamics, and Materials Conference, Honolulu, HI, April 2007, https://doi.org/10.2514/6.2007-1709

[37] Vos, R., Gurdal, Z. and Abdalla, M. Mechanism for warp-controlled twist of a morphing wing, *J. Aircraft*, 2010, **47**, (2).

[38] Dale, A.S., Cooper, J.E. and Mosquera, A. Adaptive camber-morphing wing using 0-v honeycomb, 54th AIAA/ASME/ASCE/AHS Structures, Structural Dynamics, and Materials Conference, Boston, MA, April 2013, https://doi.org/10.2514/6.2013-1510

[39] Molinari, G., Arrieta, A.F. and Ermanni, P. Aero-structural optimization of three-dimensional adaptive wings with embedded smart actuators, *AIAA J.*, 2014, **52**, (9), pp 1940–1951.

[40] Feifel, W.M. Combination of aileron and flap deflection for minimum induced drag roll control, *Tech. Soaring*, 1980, **5**, pp 15–23.

[41] Brincklow, J.R. and Hunsaker, D.F. Aileron size and location to minimise induced drag during rolling-moment production at zero rolling rate, *Aeronaut. J.*, 2021, London, **125**, (1287), pp 807–829.

[42] Munk, M.M. A New Relation Between the Induced Yawing Moment and the Rolling Moment of an Airfoil in Straight Motion, NACA TR-197, June 1925.

[43] Phillips, W.F. and Snyder, D.O. Modern adaptation of Prandtl's classic lifting-line theory, *J. Aircraft*, 2000, **37**, (4), pp 662–670, http://arc.aiaa.org/doi/10.2514/2.2649

[44] Phillips, W.F., Hansen, A.B. and Nelson, W.M. Effects of tail dihedral on static stability, *J. Aircraft*, 2006, **43**, pp 1829–1837.

[45] Phillips, W.F. and Alley, N.R. Predicting maximum lift coefficient for twisted wings using lifting-line theory, *J. Aircraft*, 2007, **44**, pp 898–910.

[46] Goates, C.D. and Hunsaker, D.F. Modern implementation and evaluation of lifting-line theory for complex geometries, *J. Aircraft*, 2023, **60**, (2).

[47] Reid, J.T. and Hunsaker, D.F. General approach to lifting-line theory, applied to wings with sweep, *J. Aircraft*, 2020, **58**, (2), pp 334–346, https://doi.org/10.2514/1.C035994

[48] Phillips, W.F. and Hunsaker, D.F. Lifting-line predictions for induced drag and lift in ground effect, *J. Aircraft*, 2013, **50**, pp 1226–1233, https://doi.org/10.2514/1.C032152

[49] Hodson, J., Hunsaker, D.F. and Spall, R. Wing optimization using dual number automatic differential in MachUp, 55th AIAA Aerospace Sciences Meeting, American Institute of Aeronautics and Astronautics, January 2017, Grapevine, TX, http://arc.aiaa.org/doi/10.2514/6.2017-0033

[50] National Aeronautics and Space Administration, Prandtl-D Aircraft, NASAfacts, March 2016, https://www.nasa.gov/wp-content/uploads/2021/09/fs-106-afrc.pdf

[51] Callen, K. *Test and Analysis of the Mass Properties for the PRANDTL-D Aircraft*, Carthage College, 2012.

[52] Broyden, C.G. The convergence of a class of double-rank minimization algorithms, *IMA J. Appl. Math.*, 1970, **6**, (1), pp 76–90, https://doi.org/10.1093/imamat/6.1.76

[53] Fletcher, R. A new approach to variable metric algorithms, *Comput. J.*, 1970, **13**, (3), pp 317–322.

[54] Goldfarb, D. A family of variable metric updates derived by variational means, *Math. Comput.*, 1970, **24**, (109), pp 23–26.

[55] Shanno, D. Conditional of Quasi-Newton methods for function minimization, *Math. Comput.*, 1970, **24**, (111), pp 647–656.